Study of W^{±} and Z boson production in proton-lead collisions at the LHC with Kulagin-Petti nuclear parton distributions

Peng Ru, S. A. Kulagin, R. Petti, and Ben-Wei Zhang

Study of $W^{\pm}$ and Z Boson Production in Proton-Lead Collisions at the LHC with KP Nuclear Parton Distributions

Peng Ru

School of Physics & Optoelectronic Technology,

Dalian University of Technology, Dalian 116024, China[*]

S. A. Kulagin

Institute for Nuclear Research of the Russian Academy of Sciences, Moscow 117312, Russia[†]

R. Petti

Department of Physics and Astronomy,

University of South Carolina, Columbia SC 29208, USA[‡]

Ben-Wei Zhang

Key Laboratory of Quark & Lepton Physics (MOE) and Institute of Particle Physics,

Central China Normal University, Wuhan 430079, China[§]

Abstract

We present a detailed study of the (pseudo)rapidity distributions of massive vector bosons produced in p+p and p+Pb collisions at the LHC within the NLO approximation in pQCD. In particular, we discuss the impact of different cold nuclear matter effects on this process using the nuclear parton distributions calculated from the microscopic model developed by Kulagin and Petti (KP). This model was successfully applied to study nuclear effects in the deep-inelastic scattering and the Drell-Yan reactions off various (fixed) target nuclei. Results are compared with the recent CMS and ATLAS p+Pb data with $\sqrt{s} = 5.02\,\text{TeV}$ per two colliding nucleons. We found an excellent agreement between the predictions of the KP model and the recent LHC data on $W^{\pm}$ and Z^0 production in p+Pb collisions, including the differential cross sections, the forward-backward asymmetries, and W charge asymmetry. We also discuss the sensitivity of the current and future LHC data to the underlying mechanisms responsible for the nuclear modifications of PDFs.

PACS numbers: 25.75.Bh, 14.70.Fm, 14.70.Hp, 24.85.+p, 13.38.-b, 12.38.Qk

[*] pengru@mail.dlut.edu.cn

† kulagin@ms2.inr.ac.ru

‡ roberto.petti@cern.ch

§ bwzhang@mail.ccnu.edu.cn

I. INTRODUCTION

The production of massive vector gauge boson in relativistic hadron-hadron collisions has been extensively studied at pp and $p\bar{p}$ collisions at the LHC and the Tevatron and is well understood by the Standard Model (SM) in terms of perturbative quantum cromodynamics (pQCD) [1, 2]. For this reason, $W^\pm$ and Z^0 production is commonly considered as a fundamental candle for SM physics at the LHC, considering the relatively large yields due to the high center-of-mass energy and luminosity available, as well as the clean experimental signatures. The W/Z data from $pp(p\bar{p})$ collisions at the Tevatron and the LHC also provide valuable information about the parton density functions (PDF) of the nucleon in global QCD fits [3–8].

The recent precision data from the CMS [9, 10] and ATLAS [11, 12] experiments offer the possibility to extend the study of $W^\pm$ and Z^0 boson production to proton-lead collisions with $\sqrt{s} = 5.02\,\mathrm{TeV}$ per two coliding nucleons at the LHC [13–21]. Since the QCD factorization theorem [22] is expected to hold for nuclei, we can still describe this process in terms of pQCD, with the corresponding nuclear PDFs for the lead nucleus. To this end, we recall that PDFs are universal characteristics of the target at high momentum transfer Q^2, which are driven by non-perturbative strong interactions in the considered target. The leptonic decays of W/Z bosons produced through the Drell-Yan mechanism (DY) are of particular interest in this context, since they are not modified by the hot and dense medium created in the heavy ion collisions and the decay leptons pass through this medium without being affected by the strong interaction. Furthermore, the intrinsic asymmetry in the p+Pb collision system allows to probe different Pb fragmentation regions and nuclear parton kinematics by selecting different rapidity values, $e.g.$, with observables like the forward-backward asymmetries. The above considerations make the W/Z bosons production in p+Pb collisions a very good tool to study nuclear modifications of PDFs and to test the validity of the QCD factorization for nuclei. It is worth noting that the LHC data provide a unique opportunity to access the high $Q^2 \sim (100\,\mathrm{GeV})^2$ phase space region, never explored before by fixed target deep inelastic scattering (DIS), nor by other experiments.

Several phenomenological parameterizations of nuclear parton distributions (NPDF) are available in literature [23–27]. Such analyses assume separate nuclear corrections for each parton distribution, which are conventionally extracted from global fits to nuclear data

including primarily DIS and DY production. With the recent availability of data from heavy-ion collisions at RHIC and the LHC, additional data sets are included in NPDF analyses [24–26, 28, 29]. Although these QCD-based studies are useful in constraining nuclear effects for different partons, they provide limited information about the underlying physics mechanisms responsible of the nuclear modifications of PDFs. Furthermore, they result in many free parameters.

A different approach to NPDFs was introduced in Refs.[30, 33]. Nuclear PDFs are computed on the basis of an underlying microscopic model incorporating several mechanisms of nuclear modifications including the smearing with the energy-momentum distribution of bound nucleons (Fermi motion and binding), the off-shell correction to bound nucleon PDFs, the contributions from meson exchange currents and the coherent propagation of the hadronic component of the virtual intermediate boson in the nuclear environment. This model explains to a high accuracy the observed x, Q^2 and nuclear dependencies of the measured nuclear effects in DIS on a wide range of targets from deuterium to lead [30–32], as well as the magnitude, the x and mass dependence of all the available data from Drell-Yan production off various nuclear targets [33].

In this paper we perform a detailed study of the (pseudo)rapidity distributions of various observables for $W^{\pm}$ and Z^0 productions in p+Pb collisions at the LHC with the KP nuclear PDFs [30, 33]. We compare our predictions with the recent CMS and ATLAS data at $\sqrt{s} = 5.02$ TeV and discuss the impact of individual nuclear effects on the observed distributions. To this end, the KP model allows an interpretation of the experimental results in terms of the underlying nuclear physics mechanisms. We also address the flavor dependence of the nuclear modifications of PDFs in the context of both W^+ and W^- distributions. This topic is of particular interest since the CMS experiment reported possible hints of such a flavor dependence from the W charge asymmetry measured in p+Pb collisions [9].

This paper is organized as follows. In Sec.II we outline the description of massive vector boson production in the Drell-Yan process in proton-proton collisions. Section III summarizes the main features of the microscopic model used to calculate the KP nuclear PDFs. In Sec.IV we apply this model to study massive vector boson production in p+Pb collisions at the LHC. Our results are presented in Sec.V, together with detailed comparisons with the recent data from the CMS and ATLAS experiments at $\sqrt{s} = 5.02$ TeV at the LHC. In Sec. VI we summarize.

II. VECTOR BOSON PRODUCTION IN THE DRELL-YAN PROCESS

The production of massive vector bosons ($W^{\pm}$ and Z^0, denoted as V) through the DY mechanism in high-energy hadronic collisions is a well understood process within the framework of the perturbative QCD [1, 2]. The QCD factorization theorem [22] allows to express the corresponding production cross section as a convolution of the PDF in the colliding hadrons with the partonic hard-scattering cross section, which can be calculated in pQCD:

$$\frac{\mathrm{d}\sigma^{DY}_{AB \to VX \to llX}}{\mathrm{d}y} = \sum_{a,b} \int \mathrm{d}x_a \mathrm{d}x_b q_{a/A}(x_a, Q^2) q_{b/B}(x_b, Q^2) \frac{\mathrm{d}\hat{\sigma}_{ab \to VX \to llX}}{\mathrm{d}y}. \tag{1}$$

where $q_{a/A}$ denotes the PDF of flavor a in the hadron A, the sum is taken over all possible parton flavors, and $\mathrm{d}\sigma_{AB}/\mathrm{d}y$ and $\mathrm{d}\hat{\sigma}_{ab}/\mathrm{d}y$ are the hadronic and partonic differential cross sections as a function of the vector boson rapidity y. With the presence of a high-invariant-mass lepton pair ll in final state, massive vector boson production provides a clean experimental signature to study the PDFs of the hadrons involved in this process. In this paper we discuss the vector boson production cross sections focusing on $p + p$ and $p + {}^{208}\text{Pb}$ collisions at the LHC.

The partonic cross section in Eq.(1) can be calculated within pQCD order-by-order at the scale Q^2. At the leading order in the α_S expansion (LO), this cross-section is entirely determined by the quark-antiquark annihilation process (*e.g.*, $u\bar{d} \to W^+ \to l^+\nu$ or $q\bar{q} \to Z^0 \to l^+l^-$). At the next-to-leading order (NLO), additional contributions to the partonic cross-section may arise from three different kinds of processes: i) one-loop virtual gluon corrections; ii) gluon emission corrections $q\bar{q} \to Vg$; and iii) the corrections from quark-gluon scattering $qg \to Vq$ or $\bar{q}g \to V\bar{q}$ [2].

The NLO and next-to-next-to-leading (NNLO) coefficients for the partonic cross-sections of the DY process and the hadronic W and Z boson production are well known [34–39]. It should be noted that the NNLO corrections to the boson-rapidity distributions in relativistic heavy ion collisions are small at the LHC kinematics [18, 19].

Our numerical analysis is carried out mostly to the NLO approximation in pQCD using the DYNNLO program [38, 39], which is widely used to study the vector boson production at the LHC, as well as at the Tevatron. As an essential input for our calculations, we use two different proton PDF sets: ABMP15 [3] and CT10 (2012 version) [8]. The renormalization and the factorization scales are both set at the vector boson mass.

Figure 1 shows the normalized differential cross section computed for Z^0 boson production in $p+p$ collisions at $\sqrt{s} = 7$ TeV, as a function of the Z^0 rapidity. A good agreement between the NLO predictions and the CMS data [40] on Z^0 production is observed by using both the ABMP15 and the CT10 PDFs. Similarly, the DYNNLO program provides a good description of the W-boson production at the LHC [18, 19].
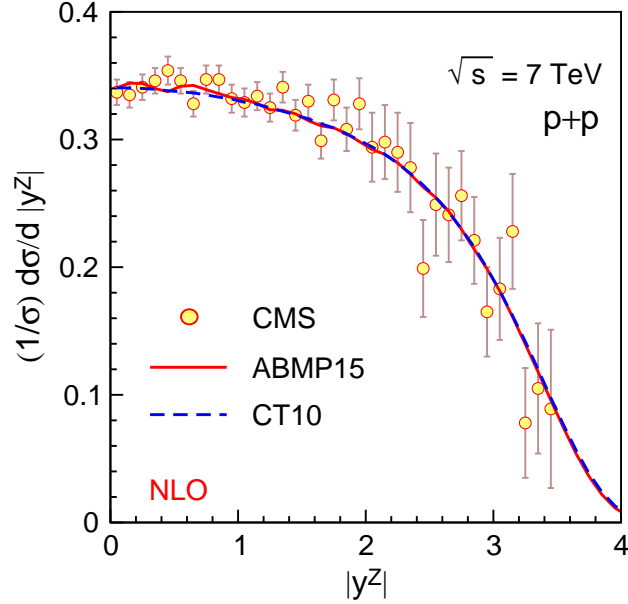

FIG. 1. Normalized differential cross section for Z^0 production in p+p collisions at $\sqrt{s} = 7$ TeV as a function of the Z^0 rapidity. The data points show the CMS measurement from Ref. [40] with statistical and systematic uncertainties added in quadrature. The invariant-mass of the lepton pair is $60 < m_{ll} < 120$ GeV [40]. The curves are obtained from NLO calculations using two different PDF sets: ABMP15 [3] (solid line) and CT10 [8] (dashed line).

III.   KP NUCLEAR PARTON DISTRIBUTION FUNCTIONS

The calculation of the W/Z production cross-sections in p+A collision requires both proton and nuclear PDFs. In the present study we use the microscopic model of nuclear PDF of Refs.[30, 33] (KP model). In the following we will briefly summarize the main features of this model by using the DIS formalism in the nucleus rest frame for better clarity. However, we note that PDFs are universal Lorentz-invariant functions and therefore the results can be used to describe different processes like W/Z production in any reference

frame.

The NPDF of Ref.[33] include different contributions as follows:

$$q_{a/A} = \langle q_{a/p} \rangle + \langle q_{a/n} \rangle + \delta q_a^{\mathrm{MEC}} + \delta q_a^{\mathrm{coh}}, \tag{2}$$

where $q_{a/A}$ is the PDF of flavor a in a nucleus A (for brevity we have suppressed the explicit dependencies on x and Q^2). The first two terms on the right side stand for the contribution from the bound protons and neutrons, and the brakets denote the averaging with the nuclear spectral function. The terms $\delta q_a^{\mathrm{MEC}}$ and $\delta q_a^{\mathrm{coh}}$ are the corrections arising from nuclear meson exchange currents (MEC) and the coherent interactions of the intermediate virtual boson with the nuclear target, respectively.

The first two terms in Eq.(2) dominate in the valence region $x > 0.1$ and in the nucleus rest frame can be written as a convolution with the proton and neutron spectral function [30, 33, 41, 42]. In particular, for the proton contribution we have:

$$\langle q_{a/p} \rangle = \int \mathrm{d}\varepsilon \mathrm{d}^3\boldsymbol{p}\, \mathcal{P}_p(\varepsilon, \boldsymbol{p}) \left(1 + \frac{p_z}{M}\right) \frac{x'}{x}\, q_{a/p}(x', Q^2, p^2), \tag{3}$$

where the integration is taken over the energy ε and the momentum $\boldsymbol{p}$ of the bound (off-shell) nucleon, $\mathcal{P}_p$ is the spectral function describing the distribution over energy and momentum of bound protons in the nucleus at rest, and $q_{a/p}$ is the PDF of the bound proton with four-momentum $p = (M + \varepsilon, \boldsymbol{p})$ with M being the proton mass. The Bjorken variable of the nucleus is x and the corresponding variable of the bound proton with four momentum p is $x' = Q^2/2p \cdot q = x/[1 + (\varepsilon + p_z)/M]$ (the z axis in Eq.(3) is antiparallel to the direction of the momentum transfer $\boldsymbol{q}$). A similar expression can be written for the bound neutron term in Eq.(2). For brevity, we dropped $1/Q^2$ terms in Eq.(3) (for more detail see Ref.[33]).

Note that Eq.(3) was obtained starting from a Lorentz-covariant approach and using a systematic expansion of matrix elements in series of the small parameters $\boldsymbol{p}/M$ and ε/M, keeping terms of the order $\boldsymbol{p}^2/M^2$ and ε/M [30, 41, 42]. The integrand in Eq.(3) factorizes into two terms involving the contribution from two different scales: i) the nuclear distribution $\mathcal{P}$ describing the processes at the nucleon level in the nuclear ground state, and ii) the PDF $q_{a/p}$ or $q_{a/n}$ describing the processes at the parton level in the nucleon. The proton (neutron) spectral function in Eq.(3) is normalized to the proton (neutron) number in the nucleus. This normalization condition also ensures the proper normalization of the nuclear valence PDF by Eq.(3). In applications we use a model spectral function, which includes both a mean field

contribution dominant at low energy and momentum, and a high-momentum contribution related to short range nucleon-nucleon correlations [30].

The off-shell nucleon PDF in Eq.(3) explicitly depends on the nucleon invariant mass squared p^2. Since the characteristic momenta of a bound nucleon are small compared to its mass, the integration in Eq.(3) covers mainly covers a region in the vicinity of the mass shell and the nucleon virtuality $v = (p^2 - M^2)/M^2$ can be considered a small parameter. We can then expand the PDF in series of v, keeping only the leading term [30, 33, 42]:

$$q_{a/p}(x, Q^2, p^2) = q_{a/p}(x, Q^2) \left[1 + \delta f(x, Q^2) \, v \right], \tag{4}$$

$$\delta f(x, Q^2) = \partial \ln q_{a/p}(x, Q^2, p^2)/\partial \ln p^2, \tag{5}$$

where $q_{a/p}$ in the right side of Eq.(4) is the PDF of the on-mass-shell proton (or neutron) and the derivative is evaluated on the mass shell $p^2 = M^2$.

The off-shell (OS) function δf can be regarded as a special nucleon structure function, which describes the relative modification of nucleon PDF in the vicinity of the mass shell. This function does not contribute to the cross sections of the on-mass-shell nucleon, but it is relevant only for the bound nucleon and describes its response to the interaction in a nucleus. In general, the function δf may depend on the PDF type and may be different for protons and neutrons. However, a detailed analysis of data on the ratios of DIS structure functions [30, 32] and of DY cross sections [33] for different nuclei supports the hypothesis of a universal OS function for all nucleon PDFs, with no significant Q^2 dependence, *i.e.* $\delta f(x, Q^2) = \delta f(x)$. The results of Ref.[30] on δf are also supported by a recent combined analysis of DIS data off proton and deuteron targets, Drell-Yan production in pp and pD interactions, and $W^\pm$ and Z boson production in pp and $p\bar{p}$ collisions [43]. Therefore, we use a single universal off-shell function $\delta f(x)$ in computing all NPDFs.

The mesonic fields mediate the nucleon-nucleon interaction at distances exceeding the typical nucleon size and also contribute to the quark-gluon content of the nucleus. The nuclear correction δq_a^{MEC} in Eq.(2), originating from DIS off the virtual mesons exchanged between bound nucleons, can be written in terms of the convolution [30, 33]:

$$\delta q_a^{\text{MEC}} = \sum_{m=\pi, \rho, \dots} f_{m/A} \otimes q_{a/m} \tag{6}$$

where the sum is taken over the possible meson states, $f_{m/A}$ is the light-cone distribution of the meson m in the nucleus A, and $q_{a/m}$ is the parton distribution of flavor a in the virtual

meson m. The meson light-cone distribution $f_{m/A}$ is calculated in Refs.[30, 33] by using the nuclear light-cone momentum balance equation between bound nucleons and meson fields, as well as the equation of motion for the meson fields. We use the pion parton distribution functions from Ref.[44] to model the virtual meson PDF $q_{a/m}$ in Eq.(6). The MEC correction results in some enhancement of the nuclear sea-quark distribution and its contribution is relevant in the region $x < p_F/M \sim 0.3$, where p_F is the nuclear Fermi momentum.

The last term in Eq.(2) is due to the propagation of the intermediate hadronic states of a virtual boson in the nuclear environment. We address this effect by replacing the sum over the set of all intermediate hadronic states by a single effective state and by describing its interaction with the nucleon with an effective scattering amplitude [30]. It is convenient to discuss coherent nuclear effects in terms of PDF combinations of definite C-parity $q^{\pm} = q \pm \bar{q}$ and, for light quarks, of definite isospin $q_0 = u + d$ (isoscalar) and $q_1 = u - d$ (isovector). For example, for the C-even isoscalar PDF combination we have:

$$\delta q_0^{\text{coh}} = q_{0/N} \ \text{Im} \, \mathcal{T}^A(a_0^+)/\, \text{Im} \, a_0^+, \tag{7}$$

where a_0^+ is the C-even isoscalar forward effective scattering amplitude off the nucleon and $\mathcal{T}^A$ is the sum of the nuclear multiple-scattering series for the effective nuclear amplitude in the corresponding channel. A detailed discussion of other PDF combinations can be found in Ref.[33].

The term δq_a^{coh} is relevant at low x and its strength is governed by the effective amplitudes a_I^C with different C-parity and isospin I. In the region of small x this correction is negative, giving rise to the nuclear shadowing (NS) effect, while in the transition region $x > 0.05$ the correction may be positive for some I and C channels, because of a constructive interference between the amplitudes a_I^C from different channels [33].

We note that different nuclear effects in different kinematical regions of x are related by the DIS sum rules and normalization constraints. In Ref.[30, 33] these conditions are treated as dynamical constraints. For example, as discussed above, the nuclear light-cone momentum sum rule at the hadronic level (nucleons and mesons) links the nucleon and meson distribution functions. The same sum rule at the partonic level constrains nuclear effects in the gluon distribution. The normalizations of the isoscalar and the isovector valence quark distributions (the baryon number and the Adler sum rules, respectively) link the coherent and the off-shell corrections, since the other contributions cancel out explicitly [33]. In

9

Ref.[30], the off-shell effect provides an explicit mechanism to cancel a negative nuclear shadowing contribution to the normalization of the nuclear valence quarks. We also use the DIS sum rules to obtain the amplitudes a_I^C in terms of the off-shell function δf and the bound nucleon virtuality v averaged with the nuclear spectral function $\mathcal{P}$ in the corresponding isospin state I.
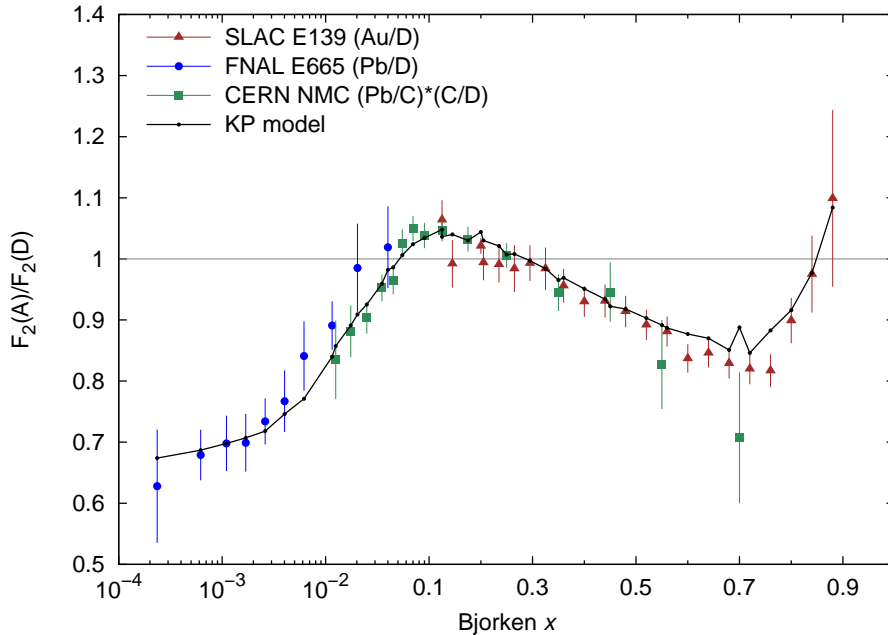

FIG. 2. Summary of data on $F_2(\text{Lead})/F_2(\text{Deuterium})$ and $F_2(\text{Gold})/F_2(\text{Deuterium})$ from the SLAC E139 [45], FNAL E665 [46], and CERN NMC [47] experiments (for NMC we show the product of the ratios Lead/Carbon and Carbon/Deuterium). The dots connected by the solid line are the predictions of Ref. [30] computed for the published values of (x, Q^2) of each data point (the wiggles are caused by different values of Q^2 for the CERN NMC and the SLAC E139 experiments). We use a logarithmic scale for $x < 0.1$ and a linear scale for $x > 0.1$ for a better display of both the small x and the large x regions.

A thorough analysis of data on the ratios of DIS structure functions off different nuclei was carried out in Ref.[30] in the context of the described model. The OS function δf, introduced in Eq.(4), was determined phenomenologically from this analysis with an approach similar to the one used for the other nucleon structure functions. The model demonstrated an excellent performance and was able to describe the observed x, Q^2 and A dependencies of data to a high accuracy. Figure 2 summarizes the DIS data on ^{208}Pb and ^{197}Au – the nuclei

10

relevant for the present study – together with the corresponding predictions of Ref.[30]. The predictions of Ref.[30] were further verified [32] with the recent nuclear DIS data from the HERMES experiment at HERA [48] and the E03-103 experiment at JLab [49]. Furthermore, the same NPDF model describes well the magnitude, the x and mass dependence of the DY production cross section off various nuclear targets [33] in the E772 [50] and E866 [51] experiments at Fermilab.

Below we summarize briefly the main features of the KP nuclear PDFs. For a nucleus of Z protons and N neutrons and $A = Z + N$ we define the ratio:

$$R_a^A(x, Q^2) = \frac{q_{a/A}(x, Q^2)}{Z q_{a/p}(x, Q^2) + N q_{a/n}(x, Q^2)}, \tag{8}$$

where $q_{a/A}$ is the nuclear PDF of flavor a, and $q_{a/p}$ and $q_{a/n}$ are the corresponding PDFs for the free proton and neutron, respectively. We assume the conventional isospin symmetry for the proton and neutron PDFs ($u_p = d_n$ and $d_p = u_n$). Figure 3 illustrates the ratios defined in Eq.(8) for different combinations of PDFs in the lead nucleus at $Q^2 = m_Z^2$ (from top to bottom): (a) nuclear correction $R_{\rm val}^{\rm Pb}$ for the valence quarks $u_v + d_v$; (b) nuclear correction $R_{\rm sea}^{\rm Pb}$ for the full antiquark distribution $\bar{u} + \bar{d} + \bar{s} + \bar{c} + \bar{b}$; (c) ratio $R_u^{\rm Pb}/R_d^{\rm Pb}$ related to the isospin-dependent nuclear effects on u and d quarks; and (d) the ratio $R_{\bar{u}}^{\rm Pb}/R_{\bar{d}}^{\rm Pb}$ for the corresponding anti-quarks. For comparison we also show the corresponding nuclear correction ratios obtained from the EPS09 phenomenological parameterization of NPDFs [24].

Figure 3 shows that the magnitude and the shape of the nuclear corrections is different for the nuclear valence and sea-quark distributions. In the region $x \ll 0.1$, the NPDFs are suppressed by the nuclear *shadowing* effect (negative $\delta q^{\rm coh}$ term). However, the magnitude of this correction is not universal and differs for the valence and sea quark distribution [30, 33]. We note that the result of the convolution of the nucleon PDF with the nuclear spectral function in Eq.(3) depends upon the shape of the nucleon PDF considered. In the small x region this correction is positive for the valence quarks, thus reducing the effect of the shadowing from the $\delta q^{\rm coh}$ term, but is negative for the sea quarks. However, the MEC correction for the sea quarks is positive, resulting in a partial cancellation between different effects. In the intermediate region $x \sim 0.1$ (usually referred as *antishadowing* region) we observe an interplay of different nuclear corrections. For the the sea quark distributions we find an almost exact cancellation between different nuclear corrections, while for the valence quarks we obtain a moderate enhancement, which is caused by the interference between
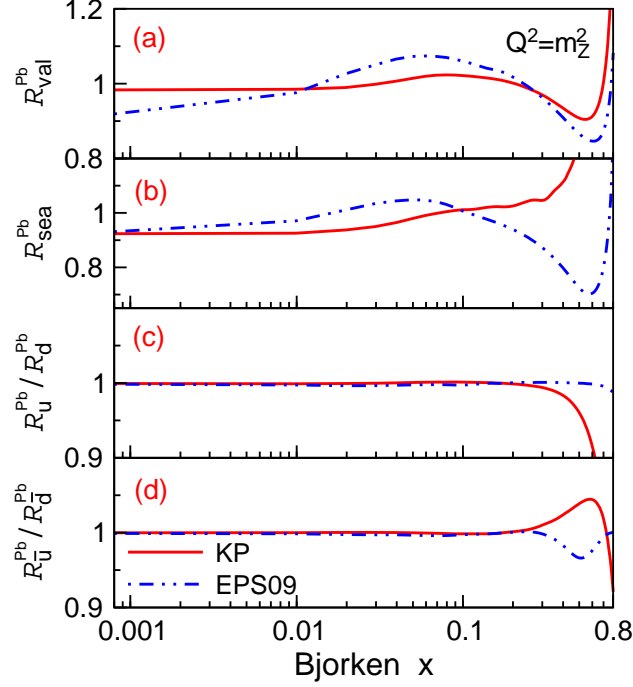
11

FIG. 3. Nuclear PDF ratios from Eq.(8) computed following Ref.[33] for ^{208}Pb at $Q^2 = m_Z^2$ as a function of the Bjorken x (solid line). The different panels (top to bottom) show the nuclear corrections for various PDF combinations: (a) valence quark distributions; (b) antiquark distributions; (c) ratio R_u^{Pb}/R_d^{Pb}, and (d) ratio $R_{\bar{u}}^{Pb}/R_{\bar{d}}^{Pb}$. The results of Ref.[24] are also shown for comparison.

the a_0^+ and a_0^- amplitudes in the multiple scattering correction [30, 33]. At large $x > 0.2$ nuclear PDFs are dominated by the incoherent scattering from bound nucleons in Eq.(3). For the valence quarks, the interplay between the Fermi motion and nuclear binding correction (FMB) and the off-shell correction results in a pronounced *EMC-effect* at large x [30, 41, 52]. The relative size of this correction strongly depends on the particular x dependence of the input nucleon PDFs. For this reason the ratios R_{val} and R_{sea} are quite different at large x, as shown in Fig.3.

The last two panels in Fig.3 illustrate the isospin (flavor) dependence of the nuclear correction factors. For the ratio R_u/R_d the model of Ref.[33] predicts

$$\frac{R_u}{R_d} = 1 + 2\frac{Z-N}{A}\left(\frac{u-d}{u+d}\right)\frac{R_1-R_0}{R_0}, \tag{9}$$

where u and d represent the PDFs of the corresponding quarks at the given (x, Q^2) kinematics, and R_0 and R_1 are the nuclear corrections from Eq.(8) for the isoscalar $q_0 = u + d$ and the isovector $q_1 = u - d$ PDF combinations, respectively. A similar expression can be

12

written for the double ratio of antiquark PDFs, $R_{\bar{u}}/R_{\bar{d}}$, with u and d replaced by $\bar{u}$ and $\bar{d}$, respectively (for more details, see Ref.[33]). We note that the magnitude of $R_u/R_d - 1$ appears to be significant only at large $x > 0.3$, where the last two factors become of the order of unity.

It is instructive to compare the nuclear effects on PDFs in Fig.3 with those on the structure function F_2 shown in Fig.2. The most visible difference is a more pronounced shadowing correction at small x for F_2 in DIS. This effect can be explained with the strong Q^2 dependence of the effective cross section $(\text{Im}\,a_0^+)$ describing the nuclear interaction in Eq.(7), since the results in Fig.3 are obtained at $Q^2 = m_Z^2$, while the data in Fig.2 have $Q^2 \sim 1\,\text{GeV}^2$ or lower. We also note that higher-twist terms (HT) as well as target mass corrections (TMC) [53] play a significant role in the results shown in Fig.2 (see Ref.[30] for more details).

IV. $W^{\pm}/Z^0$ PRODUCTION IN $p + Pb$ COLLISIONS

The rapidity distributions of $W^{\pm}/Z^0$ bosons produced in nuclear collisions at the LHC offer an excellent tool to study the cold nuclear medium effects on the (anti)quark parton distributions [13, 15, 16, 18, 19]. The corresponding LO partonic processes are indeed initiated by quarks and antiquarks, while gluons contribute only through higher order corrections to the sub-process cross sections. The analysis of the nuclear modifications on the boson rapidity distributions in p+Pb collisions is relatively simple compared to Pb+Pb collisions, since the nuclear partons are associated to a single nucleus traveling in a definite direction. Assuming the longitudinal axis along the proton beam direction, the relations between the boson rapidity y and the momentum fraction carried by a parton from the proton or the lead nucleus can be written in the LO approximation as

$$x_p = \frac{m_V}{\sqrt{s_{NN}}}e^y, \qquad x_{Pb} = \frac{m_V}{\sqrt{s_{NN}}}e^{-y}. \tag{10}$$

From Eq.(10) one can estimate the typical momentum fraction carried by the nuclear partons as $x_0 = m_V/\sqrt{s_{NN}} \sim 0.017$ at the central rapidity $y \sim 0$. If we neglect the contribution of nuclear gluons from higher order QCD corrections, x_0 corresponds to the nuclear momentum fraction carried by (anti)quarks, with the exception of the very forward region in which nuclear partons move rather slowly. The kinematic region around $x_{Pb} \sim x_0$ corresponds to

the transition between the valence-dominated and the sea-dominated regions. As a result, both the valence and the sea quark distributions play an important role in the study of $W^\pm/Z^0$ bosons produced in nuclear collisions at the LHC [18, 19]. Furthermore, bosons produced in the backward rapidity region ($y < 0$, the direction of the lead beam) can provide valuable information on the nuclear valence quark distributions, while the nuclear sea quark distributions may play a dominant role in the nuclear modifications observed in the forward rapidity region ($y > 0$, the direction of the proton beam).

Experimentally, it is easier to measure the pseudo-rapidity of the charged lepton origi-nated from the W decay, η^l, rather than the W boson rapidity, due to the additional smear-ing introduced by the undetected neutrino present in the final state. The two variables are correlated and provide similar insights on the parton distributions [15].

In addition to the differential cross-sections of massive vector bosons, observables defined as ratios of event rates are of particular interest, like the forward-backward asymmetry $R_{FB}(y)$ and the W charge asymmetry $\mathcal{A}(\eta^l)$:

$$R_{FB}(y) = \frac{N(+y)}{N(-y)}, \tag{11}$$

$$\mathcal{A}(\eta^l) = \frac{N^+(\eta^l) - N^-(\eta^l)}{N^+(\eta^l) + N^-(\eta^l)}, \tag{12}$$

where y is replaced with η^l for W boson production. These ratios can enhance the sensitivity of various observables to the parton distributions and their nuclear modifications, due to the partial cancellation of uncertainties in theoretical calculations (*e.g.*, scale dependence) and experimental measurements (*e.g.*, integrated luminosity) [9, 10, 15]. In particular, the Z^0 forward-backward asymmetry from Eq.(11) is sensitive to the ratio of small-x (sea-quark dominated) to large-x (valence-quark dominated) NPDFs, while the W charge asymmetry in Eq.(12) can shed light on the flavor dependence of the nuclear modifications of PDFs (*e.g.*, R_u vs. R_d and $R_{\bar{u}}$ vs. $R_{\bar{d}}$) [9].

The discussion of $W^\pm$ and Z production in $p + A$ collisions clearly requires to address a number of cold nuclear matter (CNM) effects affecting the PDFs of the colliding nucleus. A standard approach to calculate the W/Z production cross sections is to apply Eq.(1) with the corresponding nuclear PDFs (NPDFs) [14–21, 54–56]. A number of phenomenological NPDF parametrizations are available in literature [23–27]. In this work we use the KP NPDFs calculated on the basis of the microscopic model of Refs. [30, 33], which can provide

a deeper understanding of the physics mechanisms responsible for the nuclear modifications of massive vector boson productions in $p + A$ collisions (Sec.III).

In general, there is an interplay between the proton PDFs and the corresponding nuclear corrections. In the KP model the convolution term by Eq.(3) would result in different nuclear correction factors for different input proton PDF. For this reason the full calculation of nuclear PDFs described in Sec.III has to be repeated when changing the set of proton PDFs. The results shown in this paper are based on the 5-flavor NNLO proton PDF set of Ref.[3]. We note that the use of different proton PDFs requires some considerations even with other NPDFs available in literature. Since NPDFs are typically determined from global QCD fits to nuclear data, the use of a set of proton PDFs different from the one in the corresponding QCD fits may result in violations of the valence quark normalizations and momentum sum rule. Another factor to consider are the corrections beyond the leading twist approximation, such as the target mass correction (TMC) [53] and the dynamical HT terms. These power corrections can significantly affect the NPDF analyses, which are dominated by the relatively low Q^2 DIS nuclear data. For instance it is known that TMC are sensitive to the shape of the proton PDFs used.

Figure 4 illustrates the predictions for the W^+ differential cross section as a function of the charged lepton pseudorapidity computed in different approximations. From Fig.4 we conclude that the effect of NNLO correction on the partonic cross sections is rather small, being even more marginal in the forward-backward asymmetry $R_{FB}(y)$ and in the W charge asymmetry $\mathcal{A}(\eta^l)$. For this reason we use NLO partonic cross sections in the following analysis.

Fig.4 clearly indicates the importance of nuclear corrections in the process of W/Z production in p+Pb collisions at the LHC energy. In Sec.V we perform detailed comparisons of our predictions with the recent CMS data on $W^{\pm}$ production [9] and Z^0 production [10] at $\sqrt{s} = 5.02\,\text{TeV}$, as well as with the corresponding measurements from the ATLAS experiment [11, 12]. For completeness, our predictions are also compared with the results obtained using the EPS09 phenomenological NPDF parameterization [24], supplemented by the CT10 proton PDFs [7]. This choice is motivated by the fact that the CT10+EPS09 combination is widely used in the experimental studies at the LHC, including the CMS and ATLAS measurements of $W^{\pm}/Z$ production in p+Pb collisions of Refs. [9–12].
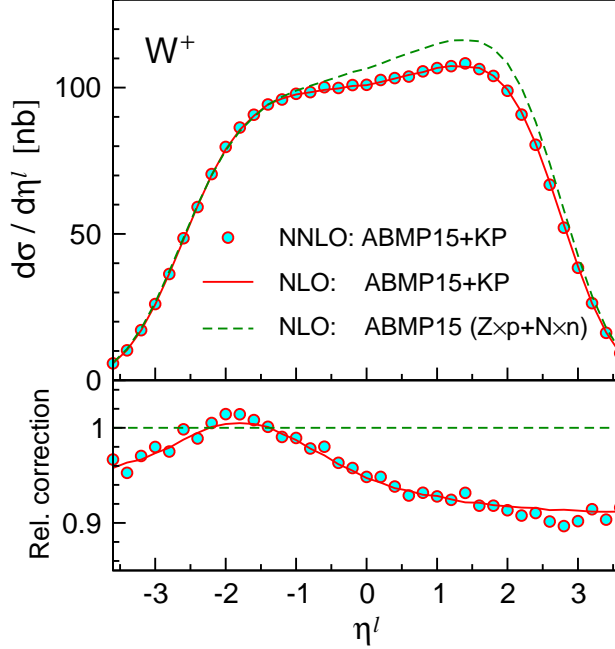
FIG. 4. Predictions for the differential cross-section of W^+ production in p+Pb collisions at $\sqrt{s_{NN}} = 5.02$ TeV using different approximations: NNLO with ABMP15+KP (solid line), NLO with ABMP15+KP (circles), and NLO with ABMP15 but with no nuclear corrections (dashed line). The bottom panel shows the corresponding ratios with respect to the results with no nuclear corrections.

V. RESULTS AND DISCUSSION

In Fig.5 we compare our results on the differential cross-sections for W^+ and W^- production in p+Pb collisions at $\sqrt{s_{NN}} = 5.02$ TeV with the CMS measurement from Ref.[9]. The cross sections are plotted as a function of the charged-lepton pseudorapidity in the laboratory frame, η_{lab}. For the CMS measurement [9] the proton and the lead beam energies are 4 TeV and 1.58 TeV/nucleon, respectively. Using these data, the relation between the pseudorapidity in the laboratory frame and that in the center-of-mass frame can easily be calculated as $\eta_{lab} = \eta_{c.m.} + 0.465$.

The precision of the recent CMS data provides some discriminating power among the theoretical predictions obtained from ABMP15+KP, CT10+EPS09, and ABMP15 with no nuclear correction. The results of the three calculations for the W^+ differential cross-section are consistent in the backward region, but display obvious differences in the forward region. The CMS data clearly favor the presence of nuclear medium effects as shown in Fig.5.
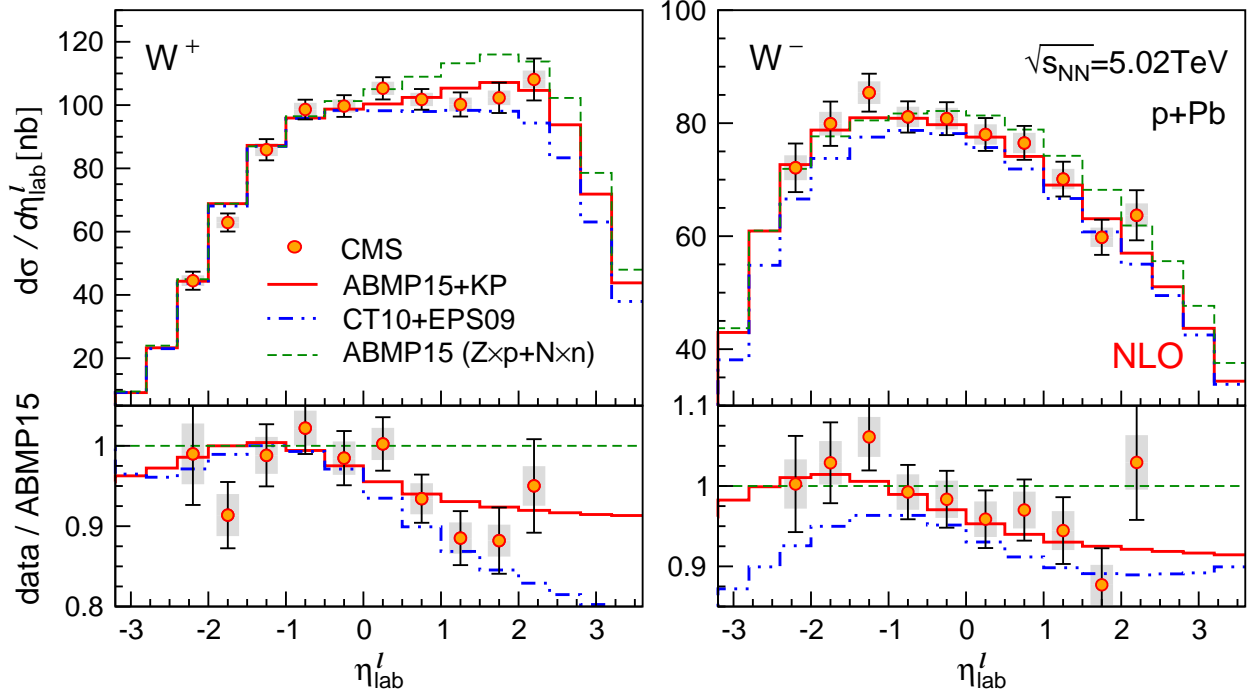
16

FIG. 5. Top panels: differential cross sections for W^+ (left) and W^- (right) production in p+Pb collisions at $\sqrt{s_{NN}} = 5.02$ TeV, as a function of the charged-lepton pseudorapidity. The data points are the CMS measurement from Ref. [9] with statistical uncertainties and total uncertainties (systematic and statistical uncertainties added in quadrature) shown as gray boxes and solid bars, respectively. The kinematic region covered corresponds to a charged-lepton transverse momentum $p_T^l > 25$ GeV/c [9]. The curves represent the predictions computed using different models: ABMP15+KP (solid), CT10+EPS09 (dashed-dotted), and ABMP15 without nuclear modifications (dashed). Bottom panels: ratios of the data (points with error bars) and the model predictions (curves) shown in the top panels with respect to the predictions with no nuclear corrections (ABMP15).

The predictions of different models for the W^- differential cross-section differ both in the backward and in the forward regions with the overall best description of the CMS data coming from the KP NPDFs. The ratios in Fig.5 indicate that the KP model predicts similar nuclear modifications (suppression) for W^+ and W^- in the forward region, but somewhat different corrections in the backward region. This behavior can be explained with the flavor dependence of the nuclear modifications in the KP model. As shown in Fig.3, the KP nuclear modifications on u and d quarks are different in the large-x (valence-
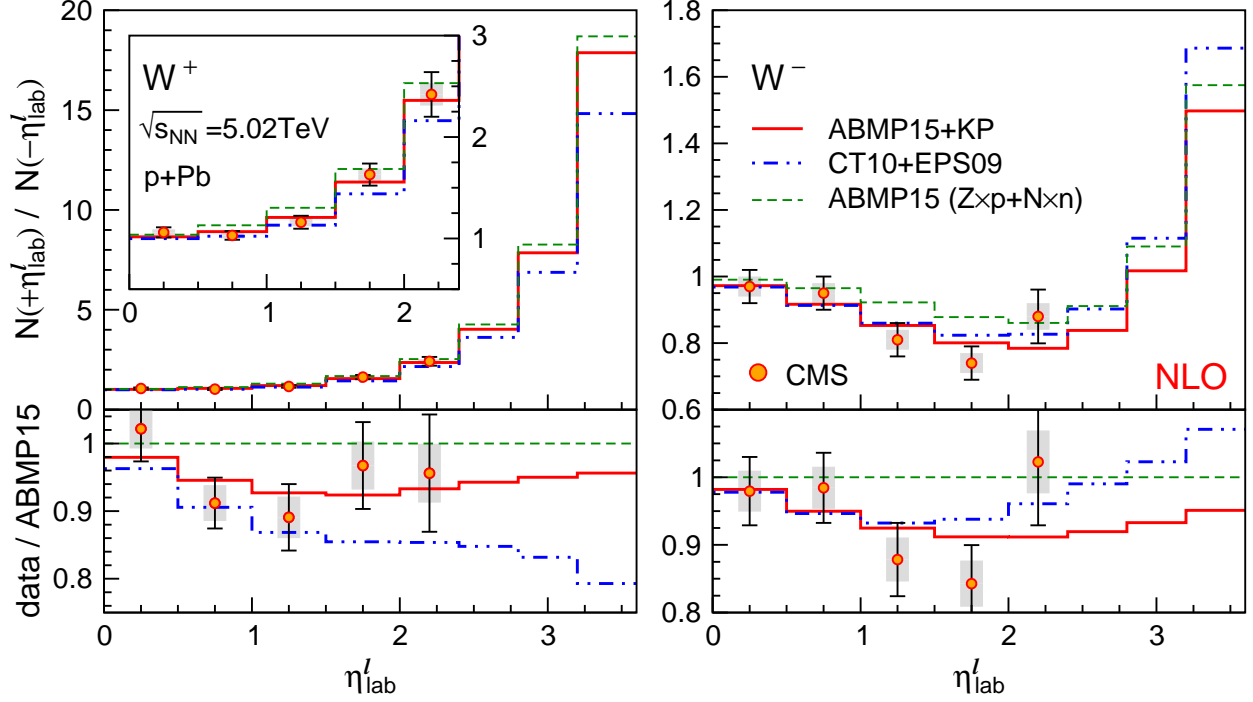
17

FIG. 6. Same notations as in Fig.5 but for the lepton forward-backward asymmetry R_{FB} for W^+ (left) and W^- (right) production in p+Pb collisions at $\sqrt{s_{NN}} = 5.02$ TeV, as a function of the charged lepton pseudo-rapidity.

quark dominated) region. Differences are also present between nuclear $\bar{u}$ and $\bar{d}$. Since the productions of W^+ and W^- are dominated by different flavors (e.g., W^+ by u and $\bar{d}$, and W^- by d and $\bar{u}$), the corresponding rapidity distributions are good observables to study the flavor dependence of nuclear modifications to PDFs. We note that different nuclear corrections for valence and sea quarks (R_{val} vs. R_{sea} in Fig.3) can also play a role in the W^+ and W^- rapidity distributions, since the W^+ and W^- production cross sections involve different fractions of valence (or sea) quarks. For instance, at LO nuclear processes intiated by valence quarks contribute about 65% to the W^+ and 75% to the W^-, at $\eta_{lab}^l \sim 2$. The different behavior of nuclear modifications in the EPS09 and KP model shown in Fig.3 plays a significant role in the difference observed on the W^+ and W^- differential cross-sections.

Our results on the forward-backward asymmetry R_{FB} for $W^\pm$ production, as a function of the charged-lepton pseudo-rapidity in the laboratory frame, are illustrated in Fig.6. This observable offers a good sensitivity to nuclear modifications of PDFs since, as discussed for the $W^\pm$ differential cross-sections, the forward and backward regions are characterized by

different nuclear corrections and parton content. The prediction with no nuclear modifications (ABMP15) does not reproduce well the W^+ nor the W^- data. Nuclear modifications are clearly needed to explain the general trend of the measured R_{FB} distributions.

In Fig.7 we show our results for the W charge asymmetry as a function of the charged-lepton pseudorapidity in the laboratory frame. The KP model predicts a small nuclear modification in the region $-3 < \eta^l_{lab} < -1.5$, due to the flavor dependence of the nuclear correction in the valence-quark dominated region (Fig. 3) and partially to the different nuclear modifications for valence and sea quarks, as discussed above. The predictions with the KP NPDFs describe very well the CMS data over the entire kinematic range. Similar results are obtained from the calculation based upon the proton PDFs ABMP15. Figure 7 also indicates that the CT10+EPS09 model predicts a rather different shape for the charge asymmetry with respect to the ABMP15+KP model. The expected values are systematically lower in the forward region and higher in the backward region, resulting in a significant overestimation of the CMS data in the region $-2 \lesssim \eta^l_{lab} \lesssim -1$ [9]. As shown in Fig.3, no significant flavor dependence is present in the EPS09 corrections, due to the initial assumption of isospin symmetry $R_u = R_d$. We note that a large part of the differences between the CT10+EPS09 and ABMP15+KP curves is related to the underlying proton PDFs used since the effect of nuclear corrections is reduced in the W-boson charged asymmetry. This partial cancellation is visible from a comparison of the curves obtained with ABMP15+KP and ABMP15 only in Fig. 7. For the effect of different proton PDFs in EPS09 see also Ref. [28]. The backward region is dominated by the valence quarks in the lead nucleus, while the forward region is related to the large-x partons in the forward going proton. Therefore, the u/d proton PDF ratio at large x is particularly relevant for the W charge asymmetry, as well as the $\bar{u}/\bar{d}$ ratio at small x.

Figure 8 summarizes our results on the differential cross section and the corresponding forward-backward asymmetry for Z^0 production in p+Pb collisions at $\sqrt{s_{NN}} = 5.02$ TeV, as a function of the Z^0 rapidity in the center-of-mass frame of the nucleon-nucleon collision. In particular, the Z^0 forward-backward asymmetry R_{FB} offers a clean probe for the study of cold medium nuclear effects [15]. The KP nuclear modifications suppress the rate of Z^0 production in the forward rapidy region and slightly enhances it in the backward rapidity region $(-2.5 < y^Z < -1.2)$. The resulting forward-backward asymmetry is therefore suppressed, similarly to the case of $W^\pm$ production. The KP model predictions are in excellent agree-
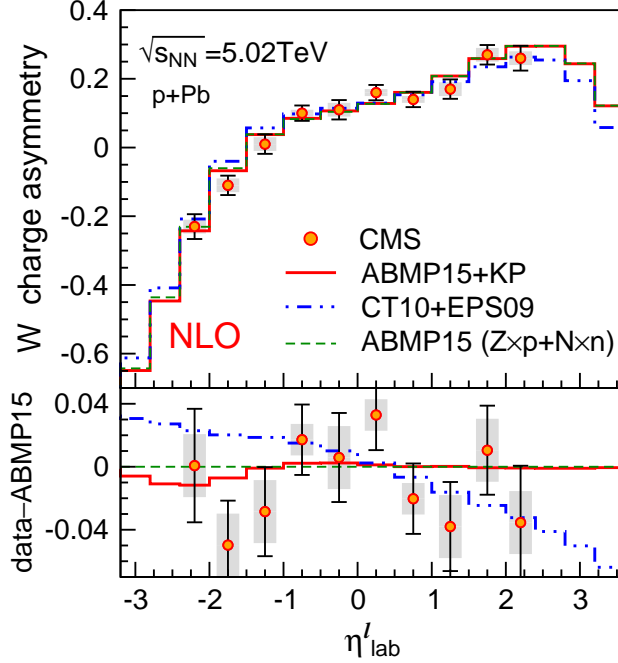
FIG. 7. Same notations as in Fig.5 but for the charge asymmetry $\mathcal{A}$ of $W^{\pm}$ produced in p+Pb collisions at $\sqrt{s_{NN}} = 5.02$ TeV, as a function of the charged lepton pseudo-rapidity. The lower panel shows the difference of data (points with error bars) and models (curves) indicated in the upper panel with respect to the predictions with no nuclear corrections (ABMP15).

ment with the CMS data for both the differential cross-section and the forward-backward asymmetry. Figure 8 shows that the results based on the ABMP15+KP model and the CT10+EPS09 parameterization are somewhat different. The difference is mainly related to the corresponding nuclear modification factors of PDFs, since our results for Z^0 production in $p+p$ collisions (see Fig.1) indicate that the ABMP15 and CT10 predictions are consistent. For the parton kinematics associated to the backward rapidity region, $0.02 < x_{Pb} < 0.1$, the EPS09 nuclear modifications at $Q^2 = m_Z^2$ lead to a stronger enhancement than the KP model for both the valence and sea quark distributions (see Fig.3). Similarly, in the region $0.001 < x_{Pb} < 0.01$, corresponding to the forward direction, the EPS09 introduces a stronger suppression of the valence quarks (see also Fig.3). As a result, the EPS09 predicts somewhat lower values for the forward-backward asymmetry with respect to the KP model.

One advantage of the KP nuclear PDFs is that they are based upon a detailed microscopic model (see Section III) allowing to disentangle the contributions from different mechanisms responsible for the nuclear modification of PDFs. In order to discuss the sensitivity of CMS
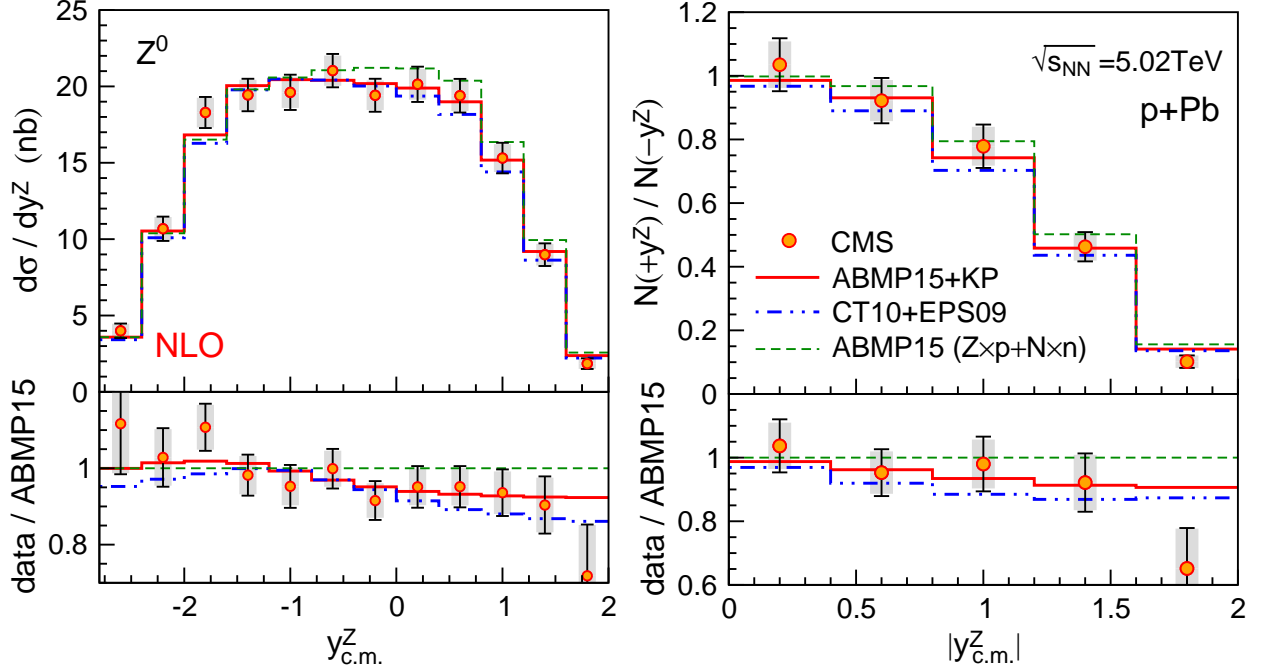
20

FIG. 8. Same notations as in Fig.5 but for the differential cross-section (left) and the related forward-backward asymmetry R_{FB} (right) for Z^0 production in p+Pb collisions at $\sqrt{s_{NN}} = 5.02$ TeV, as a function of the Z^0 rapidity. The data points are the CMS measurement [10]. The kinematic region covered corresponds a the lepton pair invariant mass $60 < m_{ll} < 120$ GeV and a lepton transverse momentum $p_T^l > 20$ GeV/c, leading to $|\eta_{lab}^l| < 2.4$ [10].

data to individual nuclear effects we define the KP nuclear modification ratio for the W/Z differential cross-sections as:

$$\mathcal{R}_{pPb}^{\mathrm{KP}}(\eta^l) = \frac{(\mathrm{d}\sigma/\mathrm{d}\eta^l)_{\mathrm{KP}}}{(\mathrm{d}\sigma/\mathrm{d}\eta^l)_{\mathrm{ABMP15}}}, \tag{13}$$

where η^l should be replaced by y^Z for Z^0 production. We evaluate this ratio using different combinations of nuclear effects in the KP model, as summarized in Sec.III: a) Fermi motion and binding correction (FMB) only; b) FMB+ off-shell correction (OS); c) FMB+OS+ coherent corrections related to nuclear shadowing (NS); and d) the complete model FMB+OS+NS+ meson exchange currents (MEC). Results are shown in Fig.9 for the W^+ and W^- differential cross-sections in p+Pb collisions at $\sqrt{s_{NN}} = 5.02$ TeV, together with the corresponding CMS data [9]. For a better understanding of the various nuclear effects at the parton level in the upper scale we also show the values of the Bjorken variable x_{Pb} obtained from Eq.(10). The relative impact of each individual nuclear effect on the
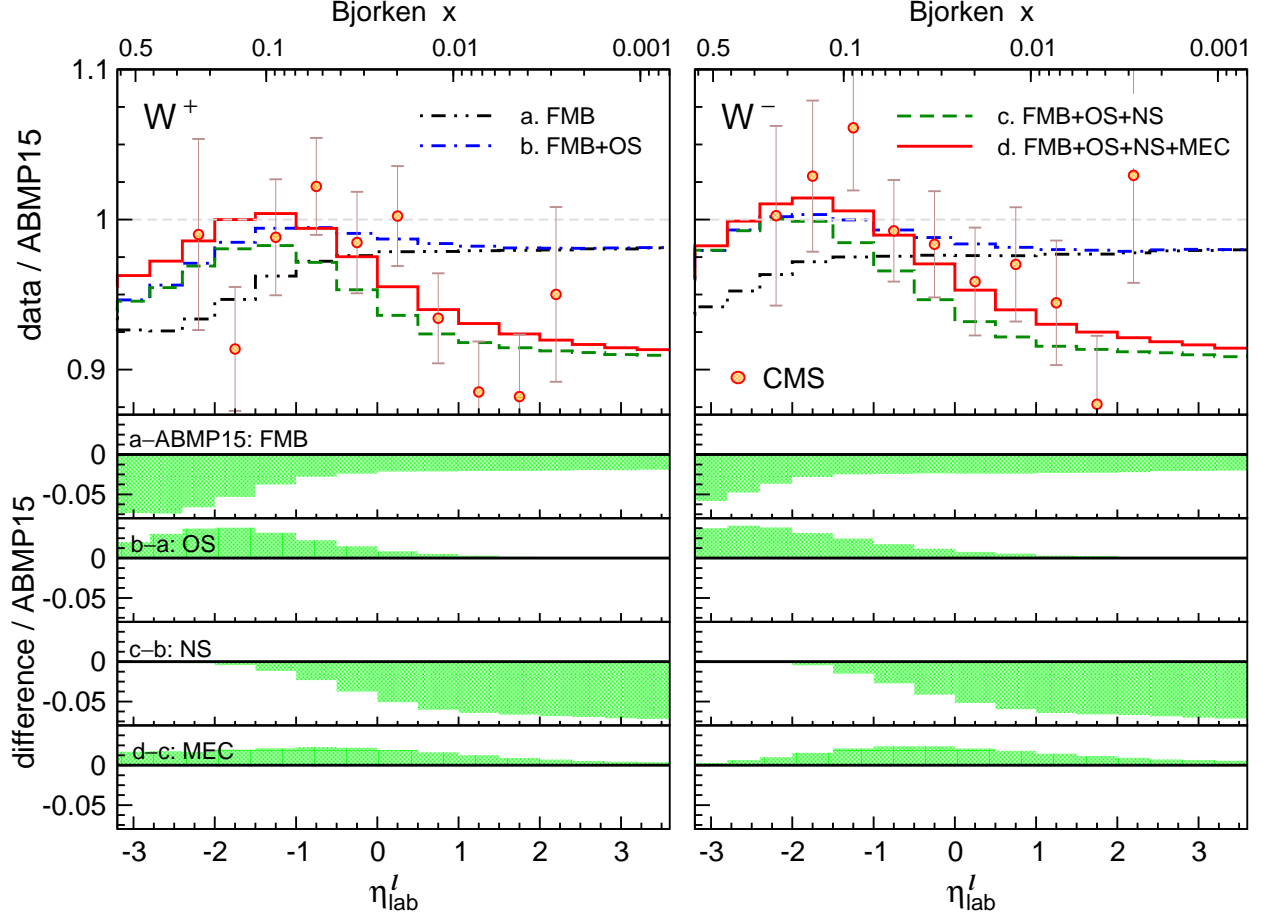
21

FIG. 9. Top panels: nuclear corrections calculated from the ratios defined in Eq.(13) for the differential cross-sections of W^+ (left) and W^- (right) production in p+Pb collisions at $\sqrt{s_{NN}} = 5.02$ TeV. The curves illustrate the impact of adding different cold nuclear matter effects in the KP model (see text for details): FMB (dashed-dotted-dotted), FMB+OS (dashed-dotted), FMB+OS+NS (dashed), and the full calculation FMB+OS+NS+MEC (solid). The data points from the CMS measurement [9] are also shown for comparison (the error bars correspond to the sum in quadrature of statistical and systematic uncertainties). A double horizontal scale is used for completeness: the bottom one shows the charged lepton pseudo-rapidity, while the top one provides an estimate of the equivalent Bjorken x_{Pb} for the partons in the lead nucleus. Bottom panels: relative contribution of each individual nuclear effect on the nuclear corrections for the W^+ (left) and W^- (right) differential cross-sections. Each contribution is obtained by subtracting the corresponding curves in the top panels, with and without the effect considered.

cross-sections can be evaluated from the difference of the ratios defined in Eq.(13) with and without the effect considered, as shown in Fig.9.

From Fig.9 we can observe that the kinematical coverage of $W^{\pm}$ production in p+Pb collisions in the CMS experiment is sensitive to all four physics mechanisms responsible for the nuclear modification of PDFs. A comparison with Fig.2 shows that in the probed region of the Bjorken x we expect significant variations in the nuclear corrections. While the size of the combined effect of FMB+OS at large x is comparable in DIS and $W^{\pm}$ production, the shadowing correction in Fig. 9 appears to be substantially reduced with respect to the nuclear DIS. This difference can be attributed to the fact that the Q^2 scale differs by 4 orders of magnitude ($Q^2 \sim 1 \, \mathrm{GeV}^2$ for fixed-target DIS in Fig. 2 and $Q^2 \sim 10^4 \, \mathrm{GeV}^2$ for Fig.3) and the corresponding effective cross sections driving the shadowing corrections at small x (see Sec.III) are significantly different [33]. As discussed in Sec.III, significant high twist contributions are also present in the low Q^2 DIS data shown in Fig. 2.
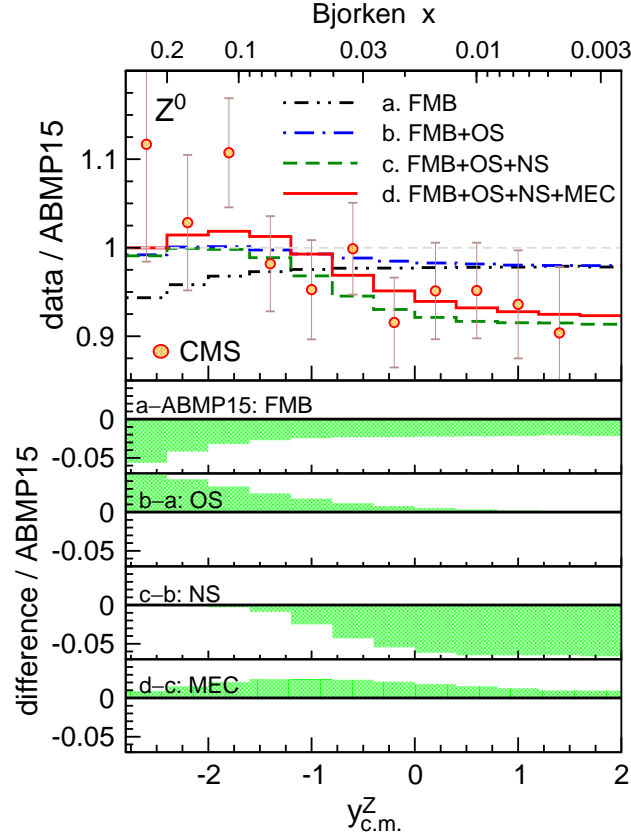

FIG. 10. Same notations as in Fig.9 but for the Z^0 differential cross-section as a function of the Z^0 rapidity. The data points indicate the CMS measurement [10].

23

The FMB and OS corrections dominate the backward region $\eta^l_{lab} < -1.5$, mainly due to their effect in the valence-quark region $x_{Pb} > 0.1$. In this rapidity region the FMB correction is negative (suppression), while the corresponding OS correction is positive (enhancement), for both W^+ and W^- production. In the forward region Fig.9 shows a suppression as a result of the nuclear shadowing on small-x partons. The enhancement observed in the intermediate and backward regions can be related to the nuclear meson correction, affecting the nuclear sea quark distributions (mainly u and d) for $x < 0.2$. It is worth noting that the shadowing corrections on W^+ and W^- production appear to be similar. Instead, differences between W^+ and W^- are observed in the nuclear corrections originated by the other physics mechanisms as a consequence of their flavor dependence ($R_u \neq R_d$, and $R_{val} \neq R_{sea}$ in Fig.3).

Figure 9 indicates that the CMS data are rather sensitive to the off-shell correction. As discussed in Sec.III, the off-shell effect plays an important role in the KP model (together with the FMB), through the off-shell structure function δf in Eq.(4). The predictions of the KP model for this study assume a single universal off-shell function for all PDFs. However, in general, this function may be flavor-dependent and different for bound protons and neutrons. A comparison of W^+ and W^- production in p+Pb collisions can potentially shed some light on these issues. The current CMS data are consistent with the assumption of a universal function, but future high precision data would be very valuable to further clarify this point.

In Fig.10 we show the contributions from different nuclear effects to the Z^0 differential cross-section in p+Pb collisions at $\sqrt{s_{NN}} = 5.02$ TeV, together with the corresponding CMS data [10]. Similar considerations can be made as for the $W^\pm$ cross-sections in Fig.9.

In the previous discussion we mainly focused on the various observables from the recent measurements by the CMS experiment. However, the ATLAS experiment also measured the W/Z [11, 12] rapidity distributions in p+Pb collisions at $\sqrt{s_{NN}} = 5.02$ TeV, although the $W^\pm$ data are still preliminary [11]. For completeness, we calculate the predictions for the differential cross-sections of W/Z production in ATLAS and compare them with the available data in Fig.11. The differences among the predictions of ABMP15+KP, CT10+EPS09, and ABMP15 with no nuclear effects for $W^\pm$ and Z^0 production in ATLAS are very similar to those discussed in the CMS context. Overall, the ABMP15+KP model predictions describe well the ATLAS data. For the Z^0 production, we observe a small excess in the data points at $-2 < y < 0$, which is not present in the CMS data shown in Fig.8.

In order to make quantitative comparisons between the various predictions and the avail-
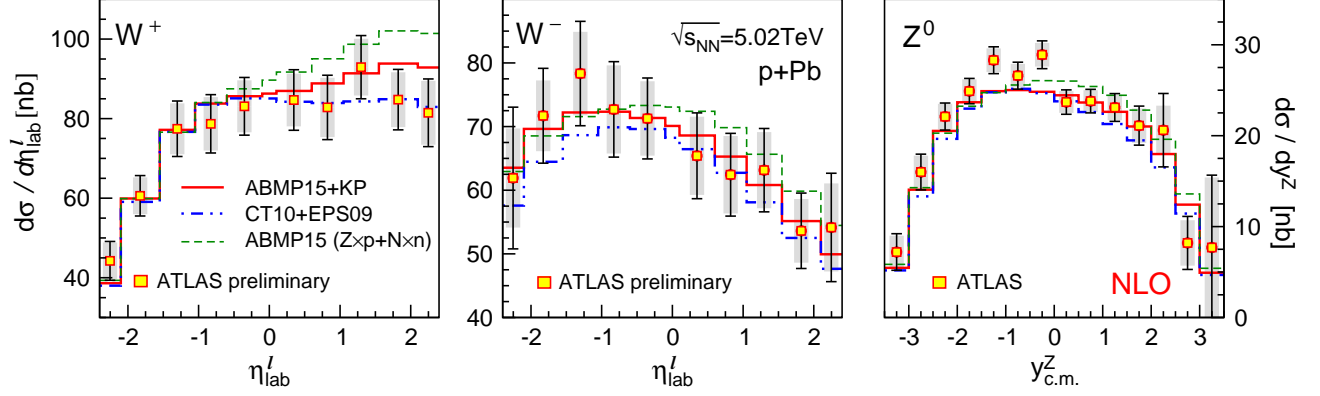
FIG. 11. Differential cross-sections for W^+ (left), W^- (middle), and Z^0 (right) production in p+Pb collisions at $\sqrt{s_{NN}} = 5.02$ TeV, as a function of the (pseudo-)rapidity. The data points indicate the ATLAS measurement of $W^\pm$ production (preliminary) [11] and the Z^0 production [12] with statistical and total uncertainties (systematic and statistical uncertainties added in quadrature) shown as gray boxes and solid bars, respectively. The kinematic region covered corresponds to a muon preudorapity $0.1 < |\eta^l_{lab}| < 2.4$, a muon transverse momentum $p^l_T > 25$ GeV/c, a neutrino transverse momentum $p^\nu_T > 25$ GeV/c, a transverse mass $m_T > 40$ GeV [11], and a Z boson invariant mass $66 < m_{ll} < 116$ GeV [12]. The curves are the predictions based on different models: ABMP15+KP (solid), CT10+EPS09 (dashed-dotted), and ABMP15 with no nuclear modifications (dashed).

able data, we evaluate the normalized χ^2 for each experimental observable as:

$$\chi^2/N_{Data} = \frac{1}{N_{Data}} \sum_{i=1}^{N_{Data}} \left[\frac{(O_{th} - O_{exp})^2}{\varepsilon^2_{stat} + \varepsilon^2_{syst}} \right]_i, \tag{14}$$

where O_{th} and O_{exp} are the theoretical prediction and the experimental measurement for the i-th data point, respectively, and ε_{stat} and ε_{syst} are the corresponding statistical and systematic uncertainties. The results obtained for the different models are summarized in Fig.12 and listed in Table I. A comparison between the normalized χ^2 values obtained with the KP NPDFs and the ones obtained without nuclear corrections (ABMP15 only) clearly shows the importance of nuclear modifications of PDFs for both CMS and ATLAS data. This observation can be interpreted as evidence for the presence of nuclear effects in W/Z production in p+Pb collisions. The predictions with KP nuclear PDFs provide the best description of both CMS and ATLAS data, with an overall value of $\chi^2/N_{Data} = 0.796$ for the combined CMS+ATLAS data set with $N_{Data} = 91$. This result demonstrates that
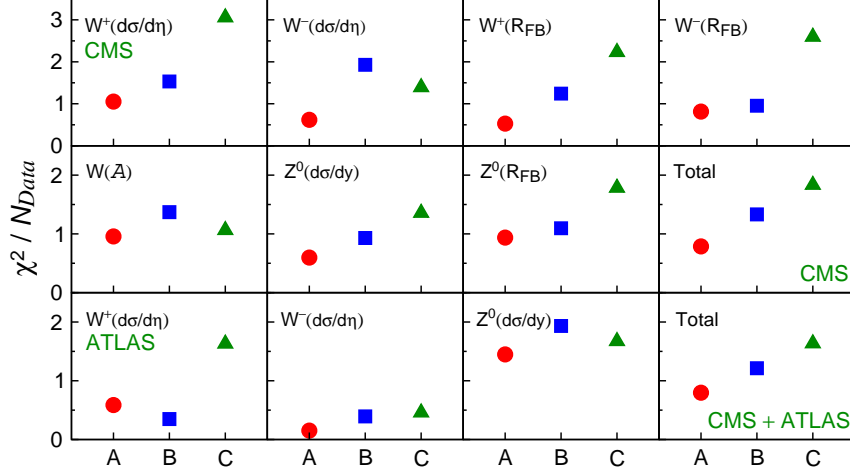
25

FIG. 12. Normalized χ^2 (per data point) for the various observables shown in the previous plots, calculated between each data set and three different model predictions: ABMP15+KP (A), CT10+EPS09 (B), and ABMP15 with no nuclear corrections (C). See Table I for more details.

the KP nuclear PDFs can be a powerful tool in the study of hard scattering processes in heavy-ion nuclear collisions. It will be interesting to extend our analysis with the KP NPDFs to other physics observables in hard scattering processes such as direct photon production [55], hadron production at large transverse momentum [57], inclusive jet [58] and di-jet productions [54], as well as gauge bosons tagged jet productions [56, 59] in both p+Pb and Pb+Pb collisions. Such studies will allow to understand how different nuclear matter effects are constrained by existing experimental measurements and to achieve a more robust separation between the initial-state cold nuclear matter effects and the final-state hot quark-gluon-plasma (QGP) medium effects in relativistic heavy-ion collisions [20, 21].

VI. SUMMARY

We performed a detailed study of the (pseudo)rapidity distributions of various observables for W/Z productions in p+Pb collisions with $\sqrt{s} = 5.02$ TeV at the LHC, using the KP nuclear PDFs together with the DYNNLO program. In this approach the nuclear modifications are computed from an underlying microscopic model including several nuclear physics mechanisms including nuclear Fermi motion and binding, off-shell correction to bound nucleon PDFs, meson exchange currents in nuclei, and coherent effects responsible for the nuclear shadowing.

TABLE I. Normalized χ^2 (per data point) for the various observables (rows) shown in the plots listed in the first column, calculated between each data set and three different model predictions: ABMP15+KP, CT10+EPS09, and ABMP15 with no nuclear corrections (last column).

Observable	N_{Data}	ABMP15 + KP	CT10 + EPS09	ABMP15 $(Zp + Nn)$
		CMS experiment:		
$d\sigma^+/d\eta^l$	10	1.052	1.532	3.057
$d\sigma^-/d\eta^l$	10	0.617	1.928	1.393
$N^+(+\eta^l)/N^+(-\eta^l)$	5	0.528	1.243	2.231
$N^-(+\eta^l)/N^-(-\eta^l)$	5	0.813	0.953	2.595
$(N^+-N^-)/(N^++N^-)$	10	0.956	1.370	1.064
$d\sigma/dy^Z$	12	0.596	0.930	1.357
$N(+y^Z)/N(-y^Z)$	5	0.936	1.096	1.785
CMS combined	57	0.786	1.332	1.833
		ATLAS experiment:		
$d\sigma^+/d\eta^l$	10	0.586	0.348	1.631
$d\sigma^-/d\eta^l$	10	0.151	0.394	0.459
$d\sigma/dy^Z$	14	1.449	1.933	1.674
CMS+ATLAS combined	91	0.796	1.213	1.635

We performed a detailed comparison between the model predictions and the recent precision data on $W^\pm$ and Z^0 productions in p+Pb collisions from the CMS and ATLAS experiments at the LHC. The data clearly favor the presence of nuclear modifications on the W/Z production cross sections with respect to the case of p+p collisions. We found an excellent agreement between the predictions based on the KP NPDFs and all the measured observables in the entire kinematic range accessible by the experiments. Our analysis of CMS and ATLAS data showed that the KP model can provide interesting insights on the underlying physics mechanisms responsible for the nuclear modifications of PDFs.

We found that the kinematics coverage of W/Z production in p+Pb collisions in the CMS and ATLAS experiments is sensitive to all underlying nuclear effects responsible for the

27

nuclear modifications of PDFs in the KP model. For this reason, the full nuclear correction on W/Z production in p+Pb collisions is the result of an interplay of different physics mechanisms. We also discussed the flavor dependence of the nuclear correction with a detailed analysis of both W^+ and W^- distributions. In particular, we found that the KP model can correctly describe the W charge asymmetry reported by the CMS experiment in p+Pb collisions.

Finally, we note that the precision currently achieved by the LHC experiments – most notably with the latest CMS measurements of $W^\pm/Z$ production – starts to be sensitive to the predicted nuclear corrections. A further improvement of the accuracy of future data sets would be extremely valuable in this context since it could allow to disentangle the effect of different underlying mechanisms responsible for the nuclear modifications of PDFs and to study their flavor dependence.

ACKNOWLEDGMENTS

[1] R. D. Field, *Applications of Perturbative QCD*, Addison-Wesley Publishing Company, 1989.

[2] R K Ellis, W J Stirling, B R Webber, *QCD and collider physics*, Cambridge University Press, 1996.

[3] S. Alekhin, J. Bluemlein, S. Moch and R. Placakyte, arXiv:1508.07923 [hep-ph].

[4] S. Alekhin, J. Blumlein, L. Caminadac, K. Lipka, K. Lohwasser, S. Moch, R. Petti and R. Placakyte, Phys. Rev. D **91**, no. 9, 094002 (2015)

[5] L. A. Harland-Lang, A. D. Martin, P. Motylinski and R. S. Thorne, Eur. Phys. J. C **75**, no. 5, 204 (2015)

[6] R. D. Ball *et al.* [NNPDF Collaboration], JHEP **1504**, 040 (2015)

[7] H. L. Lai, M. Guzzi, J. Huston, Z. Li, P. M. Nadolsky, J. Pumplin and C.-P. Yuan, Phys. Rev. D **82**, 074024 (2010)

[8] J. Gao *et al.*, Phys. Rev. D **89**, no. 3, 033009 (2014)

[9] V. Khachatryan *et al.* [CMS Collaboration], Phys. Lett. B **750**, 565 (2015)

[10] V. Khachatryan *et al.* [CMS Collaboration], Phys. Lett. B **759**, 36 (2016)

[11] The ATLAS collaboration, ATLAS-CONF-2015-056.

[12] G. Aad *et al.* [ATLAS Collaboration], Phys. Rev. C **92**, 044915 (2015)

[13] R. Vogt, Phys. Rev. C **64**, 044901 (2001)

[14] Z. Conesa del Valle, Eur. Phys. J. C **61**, 729 (2009)

[15] H. Paukkunen and C. A. Salgado, JHEP **1103**, 071 (2011)

[16] V. Guzey, M. Guzzi, P. M. Nadolsky, M. Strikman and B. Wang, Eur. Phys. J. A **49**, 35 (2013)

[17] Z. B. Kang and J. W. Qiu, Phys. Lett. B **721**, 277 (2013)

[18] P. Ru, B. W. Zhang, L. Cheng, E. Wang and W. N. Zhang, J. Phys. G **42**, no. 8, 085104 (2015)

[19] P. Ru, B. W. Zhang, E. Wang and W. N. Zhang, Eur. Phys. J. C **75**, 426 (2015)

[20] J. L. Albacete *et al.*, Int. J. Mod. Phys. E **22**, 1330007 (2013)

[21] J. L. Albacete *et al.*, arXiv:1605.09479 [hep-ph].

[22] J. C. Collins, D. E. Soper and G. F. Sterman, Adv. Ser. Direct. High Energy Phys. **5**, 1 (1988).

[23] M. Hirai, S. Kumano and T.-H. Nagai, Phys. Rev. C **76**, 065207 (2007)

[24] K. J. Eskola, H. Paukkunen and C. A. Salgado, JHEP **0904**, 065 (2009)

[25] D. de Florian, R. Sassot, P. Zurita and M. Stratmann, Phys. Rev. D **85**, 074028 (2012)

[26] K. Kovarik *et al.*, Phys. Rev. D **93**, 085037 (2016)

[27] H. Khanpour and S. Atashbar Tehrani, Phys. Rev. D **93**, 014026 (2016)

[28] N. Armesto, H. Paukkunen, J. M. Penn, C. A. Salgado and P. Zurita, Eur. Phys. J. C **76**, no. 4, 218 (2016)

[29] A. Kusina *et al.*, arXiv:1610.02925 [nucl-th].

[30] S. A. Kulagin and R. Petti, Nucl. Phys. A **765**, 126 (2006).

[31] S. A. Kulagin and R. Petti, Phys. Rev. D **76**, 094023 (2007).

[32] S. A. Kulagin and R. Petti, Phys. Rev. C **82**, 054614 (2010).

[33] S. A. Kulagin and R. Petti, Phys. Rev. C **90**, 045204 (2014)

[34] R. Hamberg, W. L. van Neerven and T. Matsuura, Nucl. Phys. B **359**, 343 (1991); Nucl. Phys. B **644**, 403 (2002).

[35] R. V. Harlander and W. B. Kilgore, Phys. Rev. Lett. **88**, 201801 (2002)

[36] C. Anastasiou, L. J. Dixon, K. Melnikov and F. Petriello, Phys. Rev. Lett. **91**, 182002 (2003)

[37] C. Anastasiou, L. J. Dixon, K. Melnikov and F. Petriello, Phys. Rev. D **69**, 094008 (2004)

[38] S. Catani and M. Grazzini, Phys. Rev. Lett. **98**, 222002 (2007)

[39] S. Catani, L. Cieri, G. Ferrera, D. de Florian and M. Grazzini, Phys. Rev. Lett. **103**, 082001 (2009)

[40] S. Chatrchyan *et al.* [CMS Collaboration], Phys. Rev. D **85**, 032002 (2012)

[41] S. A. Kulagin, Nucl. Phys. A **500**, 653 (1989).

[42] S. A. Kulagin, G. Piller and W. Weise, Phys. Rev. C **50**, 1154 (1994)

[43] S. I. Alekhin, S. A. Kulagin and R. Petti, arXiv:1609.08463 [nucl-th].

[44] M. Gluck, E. Reya and I. Schienbein, Eur. Phys. J. C **10**, 313 (1999)

[45] J. Gomez *et.al.*, Phys. Rev. D **49**, 4348 (1994).

[46] M. R. Adams *et.al.*, Z. Phys. C **67**, 403 (1995).

[47] M. Arneodo *et.al.*, Nucl. Phys. B **441**, 12 (1995); Nucl. Phys. B **481**, 3 (1996).

[48] K. Ackerstaff *et.al.*, Phys. Lett. B **475**, 386 (2000); **567**, 339(E) (2003).

[49] J. Seely *et al.*, Phys. Rev. Lett. **103**, 202301 (2009).

[50] D. M. Alde *et.al.*, Phys. Rev. Lett. **64**, 2479 (1990).

[51] M. A. Vasiliev *et.al.*, Phys. Rev. Lett. **83**, 2304 (1999).

[52] S. V. Akulinichev, S. A. Kulagin and G. M. Vagradov, Phys. Lett. B **158**, 485 (1985).

[53] H. Georgi and H. D. Politzer, Phys. Rev. **D14**, 1829 (1976).

[54] Y. He, B. W. Zhang and E. Wang, Eur. Phys. J. C **72**, 1904 (2012)

[55] W. Dai, S. Y. Chen, B. W. Zhang and E. K. Wang, Commun. Theor. Phys. **59**, 349 (2013).

[56] R. B. Neufeld, I. Vitev and B.-W. Zhang, Phys. Rev. C **83**, 034902 (2011)

[57] W. Dai, X. F. Chen, B. W. Zhang and E. Wang, Phys. Lett. B **750**, 390 (2015)

[58] I. Vitev and B. W. Zhang, Phys. Rev. Lett. **104**, 132001 (2010)

[59] W. Dai, I. Vitev and B. W. Zhang, Phys. Rev. Lett. **110**, 142001 (2013)